Short Papers

Adaptive Electromagnetic Shunt Damping

Dominik Niederberger, Sam Behrens, Andrew J. Fleming, S. O. Reza Moheimani, and Manfred Morari

***Abstract*—This paper presents a new type of passive vibration control: adaptive electromagnetic shunt damping. We propose a single-mode resonant shunt controller that adapts to environmental conditions using two different adaptation strategies. The first technique is based on minimizing the root mean square (RMS) vibration, while the second minimizes the phase difference between two measurable signals. An experimental comparison shows that relative phase adaptation performs better than the RMS technique.**

***Index Terms*—Adaptive, damping, electromagnetic, shunt.**

I. Introduction

Electromagnetic transducers [1], [2] are used extensively as actuators and sensors in vibration control [3] and vibration isolation [4], [5].

Placing an electrical impedance across the terminals of a piezoelectric transducer with a view to minimizing structural vibration is referred to as piezoelectric shunt damping [6]–[8]. In the past decade, piezoelectric shunt damping has proven a reliable alternative to active feedback control [9], [10] in applications that demand either passivity, a single transducer, or both.

In close analogy to piezoelectric shunt damping, electromagnetic shunt damping involves an electrical impedance connected across the terminals of an electromagnetic transducer [3]. The main benefits associated with electromagnetic transducers are smaller shunt voltages and larger strokes. However, alike the piezoelectric analogy, there is also a strong performance sensitivity to environmental variations [11]–[14].

To compensate for changing operating conditions, optimal performance can only be achieved by adapting the shunt online. This paper presents the concept of adaptive electromagnetic shunt damping for single mode vibration suppression. We propose a new adaptation methodology based upon controlling the relative phase difference measured between two signals. The performance of the proposed technique is compared with the traditional approach of minimizing the root mean square (RMS) vibration. At the expense of requiring an initial filter setting, relative phase adaptation is shown to tune more quickly than RMS techniques.

Manuscript received November 21, 2003; revised May 4, 2005. Recommended by Technical Editor R. Rajamani. This work supported by grants from ETH (Zurich), EMPA (Dubendorf), and ARC (Australia). The experimental facilities were provided by Laboratory for Dynamics and Control of Smart Structures (LDCSS).

D. Niederberger and M. Morari are with the Automatic Control Laboratory, ETH-Swiss Federal Institute of Technology, CH-8092 Zurich, Switzerland (e-mail: niederberger@control.ee.ethz.ch).

S. Behrens is with Australia's Commonwealth Scientific and Industrial Research Organisation (CSIRO). CSIRO Energy Centre, Mayfield West Newcastle, NSW 2300, Australia (e-mail: Sam.Behrens@csiro.au).

A. J. Fleming and S. O. R. Moheimani are with the School of Electrical Engineering and Computer Science, University of Newcastle, Callaghan 2308, Australia.

Digital Object Identifier 10.1109/TMECH.2005.859844

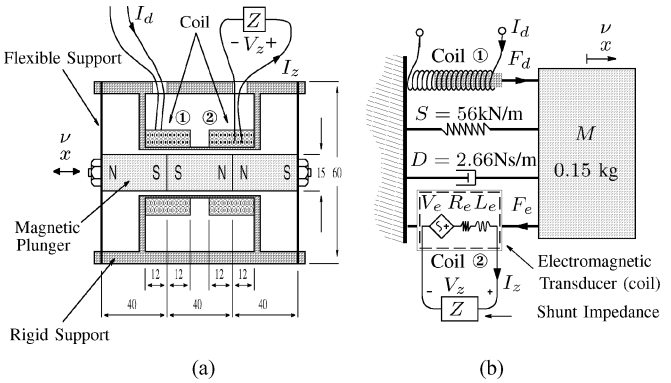

Fig. 1. (a) Side view of the experimental apparatus (all dimensions in mm). (b) Simplified model.

II. Background

A. Electromechanical Apparatus

The simple mass-spring-damper system shown in Fig. 1(a) is used to validate the proposed techniques. A simplified model of the electromechanical system is shown in Fig. 1(b). During experiments, a shunt circuit is connected to coil 2 in order to reduce vibration resulting from a disturbance force developed by coil 1. A more detailed description of the electromechanical apparatus is given in [3].

B. Modelling the Electromechanical Apparatus

The equation of motion for the electromechanical apparatus shown in Fig. 1(b), is given by

$$M\ddot{x}(t) + D\dot{x}(t) + Sx(t) = F_d(t) - F_e(t) \tag{1}$$

where $\ddot{x}(t), \dot{x}(t)$, and $x(t)$ represent the acceleration, velocity, and displacement of the mass. $F_d(t)$ is the disturbance force developed by coil 1 and $F_e(t)$ is the damping force generated by 2.

Assuming we have two ideal electromagnetic transducers in the form of conducting coils that move inside a magnetic field, we may write [1]

$$\frac{V_e}{\nu} = \frac{F_e}{I_z} = c_e \quad \text{and} \quad \frac{F_d}{I_d} = c_d \tag{2}$$

where c_e and c_d are the ideal electromechanical coupling coefficients (N/A or V/ms^{-1}). For the experimental apparatus under consideration, the coefficients are $c_e = c_d = 3.65$ N/A or V/ms^{-1} [3].

By taking the Laplace transform, we obtain

$$(Ms^2 + Cs + S)X(s) = \underbrace{c_d I_d(s)}_{F_d} - \underbrace{c_e I_z(s)}_{F_e} \tag{3}$$

which leads to the unshunted or open-loop ($F_e = 0$) transfer function from the disturbance force $F_d(s)$ to velocity $\nu(s)$

$$G_{\nu f}(s) \triangleq \left.\frac{\nu(s)}{F_d(s)}\right|_{F_e=0} = \frac{s}{Ms^2 + Ds + S} \tag{4}$$

or, from disturbance current $I_d(s)$, to velocity $\nu(s)$ with $I_z(s) = 0$

$$G_{\nu i}(s) \triangleq \left.\frac{\nu(s)}{I_d(s)}\right|_{I_z=0} = \frac{c_d s}{Ms^2 + Ds + S}. \tag{5}$$

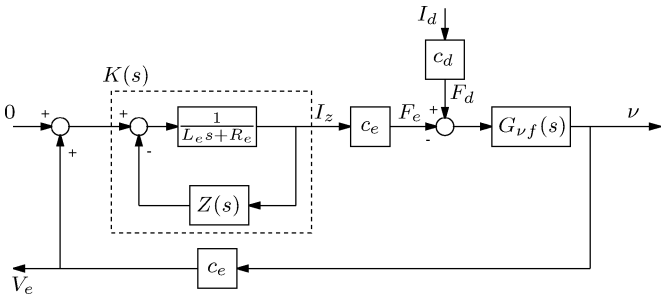

Fig. 2. Regulator feedback structure associated with electromagnetic shunt damping.

Note that $\nu(s)$ is equivalent to $sX(s)$ in the Laplace domain. In the following, preference is given to the use of $G_{\nu i}(s)$, since the current $I_d(s)$ is easier to measure than the force $F_e(s)$.

A conducting coil, as shown in Fig. 1(b), can be modeled as the series connection of an inductor L_e, a resistor R_e, and a dependent voltage source V_e [2]. The voltage source, V_e, represents the induced electromotive force (emf) that is proportional to relative velocity $\nu(s)$. The inductance and resistance of coil 2 is $L_e = 1.26$ mH and $R_e = 3.13\,\Omega$ respectively, [3]. Considering Fig. 1(b), the electrical dynamics of the shunted coil 2 is

$$V_e(s) = (Z(s) + R_e + L_e s)I_z(s). \tag{6}$$

With $V_e(s) = c_e\nu(s) = c_e sX(s)$, one obtains

$$I_z(s) = \frac{c_e sX(s)}{R_e + sL_e + Z(s)} = \frac{c_e\nu(s)}{R_e + sL_e + Z(s)} \tag{7}$$

and combining (7) with (3) results in

$$(Ms^2 + Cs + S)X(s) = c_d I_d(s) - \frac{c_e^2\nu(s)}{R_e + sL_e + Z(s)}. \tag{8}$$

From (8), the following shunted system transfer function can be obtained:

$$\tilde{G}_{\nu i}(s) = \frac{\nu(s)}{I_d(s)} = \frac{c_d G_{\nu f}}{1 + c_e^2 K(s) G_{\nu f}(s)} \tag{9}$$

where $G_{\nu f}(s)$ is defined in (4), and $K(s)$ is

$$K(s) = \frac{1}{sL_e + R_e + Z(s)}. \tag{10}$$

Note that the shunted system transfer function $\tilde{G}_{\nu i}(s)$ is equivalent in structure to a regulator feedback system where the shunt impedance $Z(s)$ parameterizes a controller $K(s)$. A block diagram representation is shown in Fig. 2. This observation enables the use of control theoretic tools to analyze the dynamics of the shunted system. In this framework, the controller parameterized by the impedance $Z(s)$ regulates the relative velocity $\nu(s)$ in response to a disturbance I_d.

III. Developing the C–R Adaptive Shunt Controllers

A. Single Mode Electromagnetic Shunt Controller

Behrens *et al.* [3] have demonstrated the effectiveness of shunting an electromagnetic transducer with a series capacitor-resistor (C–R) circuit. A single mode of vibration is heavily attenuated by tuning the C–R circuit so that an electrical resonance with the coil inductance-resistance (L_e–R_e) occurs at the frequency of mechanical resonance.

In this paper, we can apply the same methodology as suggested in the preceding. In the Laplace domain, the C–R shunt controller is

$$Z(s) = \frac{1}{Cs} + R \tag{11}$$

and according to (10), the resulting controller becomes

$$K(s) = \frac{\frac{1}{L_e}}{s^2 + \frac{R_t}{L_e}s + \frac{1}{\mathrm{CL}_e}}. \tag{12}$$

Note that the controller has a resonant structure, where $R_t = (R_e + R)$ determines the controller damping and $1/\sqrt{\mathrm{CL}_e}$ the controller resonance frequency. Optimal damping of the mechanical resonance ω_n is achieved if the C–R shunt is tuned with

$$C^* = \frac{1}{\omega_n^2 L_e}. \tag{13}$$

B. Adaptation of the Shunt Controller Capacitor

Due to variations in structural mass, stiffness, or environmental temperature, C–R shunt controllers can easily become "detuned." Significant losses in performance can easily result from relatively minor variations in the structural system. An adaptation of the C-value is needed to maintain the shunt controller tuning to the structural resonance. In the following, we describe two different adaptation techniques, and we compare their performance in Section IV.

1) RMS Adaptation: Adaptation methodologies for resonant shunt damping of piezoelectric laminated structures, using the RMS error, have been proposed in [13], [15], [16]. The RMS strain, where the piezoelectric patch is bonded, is used as the cost function to be minimized. The parameters of the shunt controller are then updated using a gradient search algorithm that minimizes the performance function.

In this section, the same adaptation technique using velocity instead of strain is applied to the electromagnetic apparatus. We choose the performance function as $E\{\nu^2(t)\}$ i.e., the objective is to minimize the RMS velocity of the mass to which coil 2 is attached. The velocity $\nu(t)$ can be estimated in real time from the shunt controller voltage and current using a simple estimator. The optimal shunt controller capacitance is then obtained from

$$C^* = \arg\min_{C>0} E\{\nu^2(t, C)\}. \tag{14}$$

This optimization problem is convex, and thus has one global solution. It can be shown that the corresponding closed loop (or shunted) system norm interpretation is

$$C^* = \arg\min_{C>0} \| \tilde{G}_{\nu i}(j\omega, C) \|_{2,S(\omega)}^2 \tag{15}$$

$$= \arg\min_{C>0} \frac{1}{2\pi}\int_{-\infty}^{\infty} S(\omega)\|\tilde{G}_{\nu i}(j\omega, C)\|_2^2\, d\omega \tag{16}$$

where $S(\omega)$ is the power spectral density of the noise excitation. Using the discrete time equivalent of $E\{\nu^2(t, C)\}$, we can approximate the performance function as

$$V^{\nu}(k, C) = \frac{1}{N}\sum_{i=kN}^{(k+1)N-1} \nu^2(iT_s, C) \tag{17}$$

where T_s is the sampling interval and N is the number of samples in each kth record interval. The required length, N, of the averaging interval can be estimated from the variance of $V^{\nu}(k, C)$. For resonant structures with frequencies around 100 Hz, excited with white noise disturbance, $(N \cdot T_s)$ is typically larger than 20 s. The parameter update is realized using a gradient search algorithm to minimize $V^{\nu}(k, C)$

$$C_{k+1} = \frac{V^{\nu}(k, C_k)(C_k - C_{k-1})}{V^{\nu}(k, C_k) - V^{\nu}(k-1, C_{k-1})}. \tag{18}$$

2) Relative Phase Adaptation: Relative phase adaptation was first proposed in [14] for the purpose of inductor-resistor (R–L) shunt damping of piezoelectric structures. The relative phase between the velocity and shunt current was controlled to $-\pi/2$ with a simple multiplication and filter operation. In [17], the concept of relative phase adaptation was extended to multimode resonant shunt circuits. A detailed convergence analysis can also be found in [17].

Consider the transfer function relating velocity $\nu(s)$ to the current $I_z(s)$ in the C–R shunt controller (see Fig. 1(b) with $V_e = c_e\nu$)

$$G_{i\nu}(s) \triangleq \frac{I_z(s)}{\nu(s)} = \frac{sc_eC}{L_eCs^2 + C(R+R_e)s + 1}. \tag{19}$$

By taking the derivative of this expression, the transfer function from the velocity $\nu(s)$ to the derivative of the current in the shunt $sI_z(s)$ becomes

$$G_{\partial i\nu}(s) \triangleq \frac{sI_z(s)}{\nu(s)} = \frac{s^2c_eC}{L_eCs^2 + C(R+R_e)s + 1}. \tag{20}$$

The phase of this transfer function is

$$\angle(G_{\partial i\nu}(j\omega)) = \tan^{-1}\left(\frac{\omega(R+R_e)/L_e}{1/(L_eC) - \omega^2}\right). \tag{21}$$

We can see that for the optimal tuning of the C–R shunt controller; i.e., $\omega_n = 1/\sqrt{L_eC}$, the phase needs to be

$$\angle(G_{\partial i\nu}(j\omega_n)) = \frac{\pi}{2}. \tag{22}$$

As shown in [14], [17], a function $f_p(C,\omega_n) = \text{sign}(\angle(G_{\partial i\nu}(j\omega_n)) - \frac{\pi}{2})$ can be defined that reveals the required tuning direction of the capacitance value, such that $\angle(G_{\partial i\nu}(j\omega_n))$ remains $\pi/2$. If C is too large, then $f_p(C,\omega_n)$ would be negative, and thus C is decreased. If C is too small, then $f_p(C,\omega_n)$ is positive and C is increased. Thus, the discrete adaptation for the kth value of C can be written as

$$C_{k+1} = C_k + \alpha \cdot f_p(C_k,\omega_n) \tag{23}$$

$$= C_k + \alpha \cdot \text{sign}\left(\angle(G_{\partial i\nu}(j\omega_n)) - \frac{\pi}{2}\right) \tag{24}$$

where α is the tuning rate. However, the calculation of the phase is complex, and, therefore, this adaptation law is of little practical use. In [14], [17], it was shown that the tuning update can be substituted with the sign of the low-pass filtered product of the two signals (here, $\nu(t)$ and $dI_z(t)/dt$), if the signals are assumed to be tonal. Since the electromagnetic shunt damping system is highly resonant, the assumption holds and the adaptation law can be formulated in the time domain as

$$\frac{d}{dt}C(t) = \beta\left(g_{\text{LP}}(t) * \left[\nu(t)\cdot\frac{d}{dt}I_z(t)\right]\right) \tag{25}$$

where $g_{\text{LP}}(t)$ is the impulse response of a low-pass filter with a cutoff frequency below $2\omega_n$, β is the tuning parameter, and $*$ denotes the time domain convolution operator. The velocity $\nu(t)$ can easily be estimated from the shunt controller voltage and current.

Due to time delays in the system, the signals $I_z(t)$ and $\nu(t)$ need to be corrected using compensators which add some additional phase lag. Compensator calibration is performed when the shunt controller is first put into service. Experiments in Section IV-B-4 show that an RMS methodology can also be used to automatically set these compensators.

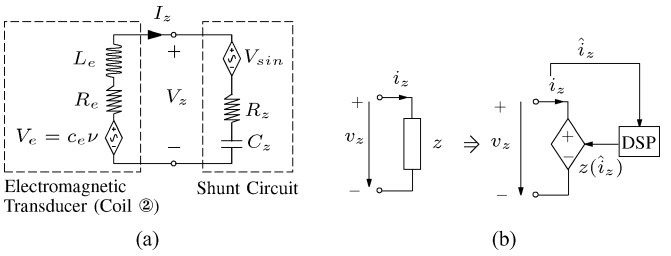

Fig. 3. (a) Electrical model of the shunted electromagnetic coil. Note $V_{\sin}$ is needed to estimate the coil resistance. (b) Synthetic impedance.

3) Adaptation of the Shunt Controller Resistor: In practical applications, the resistance of the coil is highly affected by temperature variations. Resistance variations can occur when the current flowing through the coil heats up the wire, or when the environmental temperature fluctuates. As the optimal shunt controller resistance R depends on the coil resistance R_e, the shunt controller resistance needs to be adapted online to maintain optimal performance. Moreover, estimation of the velocity requires a good estimation of the coil resistance. Therefore, an online and reliable estimation of the coil resistance needs to be provided at all times. As the signals V_z and I_z are not persistent enough and the emf voltage V_e is unknown, it is, therefore, very difficult to estimate the coil resistance from these two signals. For this reason, the resistor value is estimated using a small sinusoidal voltage excitation $V_{\sin} = \hat{V}\sin(\omega_{\sin}t)$ as demonstrated in Fig. 3(a), where the frequency $\omega_{\sin}$ is chosen to be very small (for the experiments in Section IV, $\omega_{\sin}$ was set to $2\pi\cdot 10$ rad/s), so that influence of the coil's inductance L_e, and V_e can be neglected. The nth value of the resistance is then calculated by

$$\hat{R}_e(n) = \frac{\int_{nT}^{(n+1)T} V_z^2\,dt}{\int_{nT}^{(n+1)T}(V_z\cdot I_z)\,dt} \tag{26}$$

where $T = \frac{2\pi}{\omega_{\sin}}$. In experiments, the online resistance estimator provided accurate values with low standard deviation. The measured resistance value is required for estimation of the velocity, which is in turn required by the adaptation laws. In the presence of significant temperature variation, the measured resistance is also required to correct the shunt controller resistor. For this purpose, a simple feedforward strategy is applied to obtain the nth value of the shunt controller resistor

$$R(n) = R_t^* - \hat{R}_e(n) \tag{27}$$

where R_t^* is the optimal damping resistance for the shunted system.

IV. Experimental Verification

A. Implementation of the C–R Adaptive Shunt Controller

To implement the proposed adaptive shunts, a synthetic impedance was utilized [18]. As it is illustrated in Fig. 3(b), the voltage source v_z is controlled by a function of the current i_z; i.e., $v_z(t) = z(i_z(t))$. By using the function $z(i_z(t)) = \frac{1}{C(t)}\int_0^t i_z(\tau)\,d\tau + i_z(t)R(t)$, the adaptive capacitor-resistor C–R shunt is synthesized. The synthetic impedance was chosen for its ability to change parameters and analyze signals online.

For experimental purposes, a digital signal processor (DSP) system *dSPACE*[1] was used to simulate the required function $f(i_z(t))$ in real time. Alternatively, a simple analog filter with analog adaptation circuit similar to [14] could have been used.

[1]dSPACE is a rapid prototyping digital signal processor system.

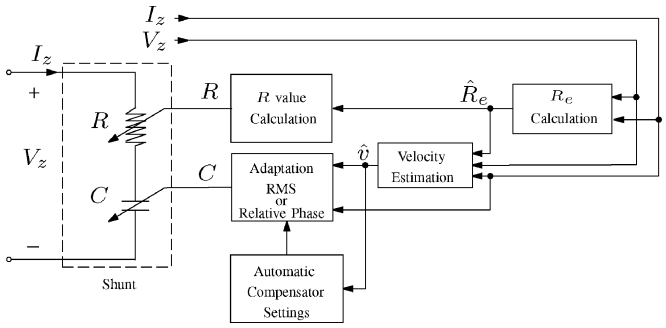

Fig. 4. Block diagram of the adaptation techniques.

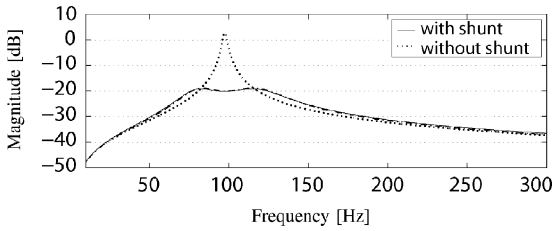

Fig. 5. Measured transfer function $G_{\nu i}$ with shunt.

B. Experimental Results

In this section, we report experiments that were carried out on the electromagnetic system described in Section II-A. Coil 2 was attached to an adaptive C–R shunt controller, whose block diagram is drawn in Fig. 4. From this figure, it can be observed that the coil resistance $\hat{R}_e$ is calculated from the shunt controller voltage V_z and current I_z, and is supplied to the velocity estimator and the optimal shunt controller resistor setting (feedforward controller). The velocity is then estimated from the shunt controller voltage V_z, current I_z, and the estimated coil resistance $\hat{R}_e$. This estimated velocity is then supplied to the adaptation law that sets the optimal shunt controller capacitance C. To perform the adaptation, either the RMS or the relative phase law is used. Notice that the block indicated as *Automatic Compensator Settings* is only used later in Section IV-B-4. The shunt controller is then implemented using the synthetic impedance circuit described in Section IV-A.

1) Nominal Performance: The damping performance of the C–R shunt controller is first experimentally verified for fixed resonance frequency ω_n and constant coil resistance R_e. The two parameters of the C–R shunt controller are calculated to be

$$C^* = \frac{1}{L_e \omega_n^2} = \frac{1}{1.26\ \text{mH} \cdot 2\pi \cdot 98\ \text{Hz}} = 2.1\ \text{mF} \tag{28}$$

$$R^* = R_t^* - R_e = -2.74\ \Omega \tag{29}$$

where R_t^* is obtained via the solution to the optimization problem proposed in [3].

The measured unshunted and shunted transferfunction from disturbance current to velocity is shown in Fig. 5. One can see that a maximal vibration suppression of 22.75 dB in velocity magnitude is achieved.

2) Step Disturbances in the Shunt Controller Capacitor: In this section, the value of the shunt capacitor C is subjected to a small detuning step change. The two proposed adaptation techniques are applied to automatically tune the C–R shunt controller back to its optimal value. Experimental results are shown in Fig. 6(a). 40 s into the experiment, the capacitor is subjected to a positive step disturbance of 4 mF. The two adaptation laws retune the C–R shunt controller back to its optimal value of 2.1 mF. The RMS adaptation requires approximately 350 s to retune the system, whereas relative phase adaptation requires only 50 s, and is hence seven times faster than the RMS method. 580 s into the experiment, the capacitor is subjected to a negative step disturbance of -1.5 mF. A similar retuning characteristic can be observed.

3) Resonance Frequency Changes: In this experiment, the resonance frequency is changed from 100 to 80 Hz by adding an extra mass to the magnetic plunger. Experimental results for RMS and relative phase adaptation are shown in Fig. 6(b). After the mass variation at 100 s, it can be observed that C is retuned to 3.2 mF. At 900 s, the resonance frequency is returned to 100 Hz and the RMS adaptation tunes C to its former value of 2.1 mF. In the second plot of Fig. 6(b), the same resonance frequency changes are shown for the relative phase controller. Here, the resonance frequency is changed at 15 s and 68 s. Note that the time scales are different.

The system response to a variation in structural resonance frequency using the relative phase technique is also shown in Fig. 7. Subfigure 1 shows the magnitude frequency response without any shunt controller; i.e., the open-loop response. In the second subfigure, the perfectly tuned shunt controller is attached to coil 2. Then, in subfigure 3, an additional mass is attached to the plunger, resulting in de-tuning. Subfigures 4 and 5 show the adaptation of the shunt controller. In subfigure 5, the shunt controller is optimally tuned to the new resonance frequency. In subfigure 6, the mass is removed and the resonance frequency returns to its initial value. The shunt is retuned in subfigures 7 to 9.

4) RMS Adaptation for the Compensator of the Relative Phase Adaptation: As explained in Section III-B-2, relative phase adaptation requires the setting of a delay compensator. This can be performed manually when the system is brought into service, or performed online using an RMS methodology similar to the RMS adaptation of C in Section III-B-1. This technique is shown in Fig. 4 where the *Automatic Compensator Setting* block minimizes the estimated velocity $\hat{v}$. An experimental example of automatic compensator tuning is shown in Fig. 8. The time constant of the RMS adaptation is chosen to be very long. At the beginning, the compensator delay for ν is suboptimal (0.265 ms instead of 0.295 ms), and the relative phase adaptation tunes C to an incorrect value (2.24 mF instead of 2.1 mF). After 2000 s, the optimal compensator delay of 0.295 ms is achieved. At time step 3400 s, the shunt capacitor is subjected to a step disturbance. With the optimally tuned compensators, the relative phase adaptation retunes C to its optimal value of 2.1 mF. The estimation of the coil resistor R_e is shown in Fig. 8, lower plot. The value is accurate even when the system is subject to disturbances.

V. Conclusion

Electromagnetic shunt damping is a technique similar in nature to piezoelectric shunt control. A tuned C–R shunt impedance connected to the terminals of a structurally attached electromagnetic transducer can reduce vibration in the host structure by greater than 20 dB. One of the characteristics of resonant shunt circuits is that performance is highly sensitive to variations in the structural resonance frequency.

In this paper, an adaptive C–R shunt controller was proposed to provide performance robustness to changing operating conditions. The shunt capacitance is adapted using two different methodologies: 1) minimizing the RMS value of the velocity using a gradient search algorithm (RMS adaptation) and 2) by controlling the relative phase between the velocity and the shunt current derivative (relative phase adaptation). As the coil resistance is highly variable due to periods of high current, the shunt resistance is also adapted using a simple feedforward controller.

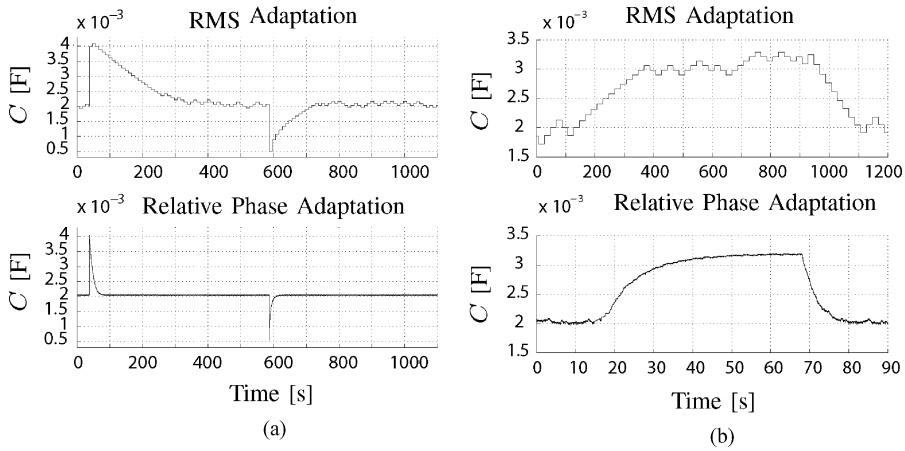

Fig. 6. (a) Step disturbances in the shunt controller capacitor. (b) Modal frequency changes by adding an additional mass.

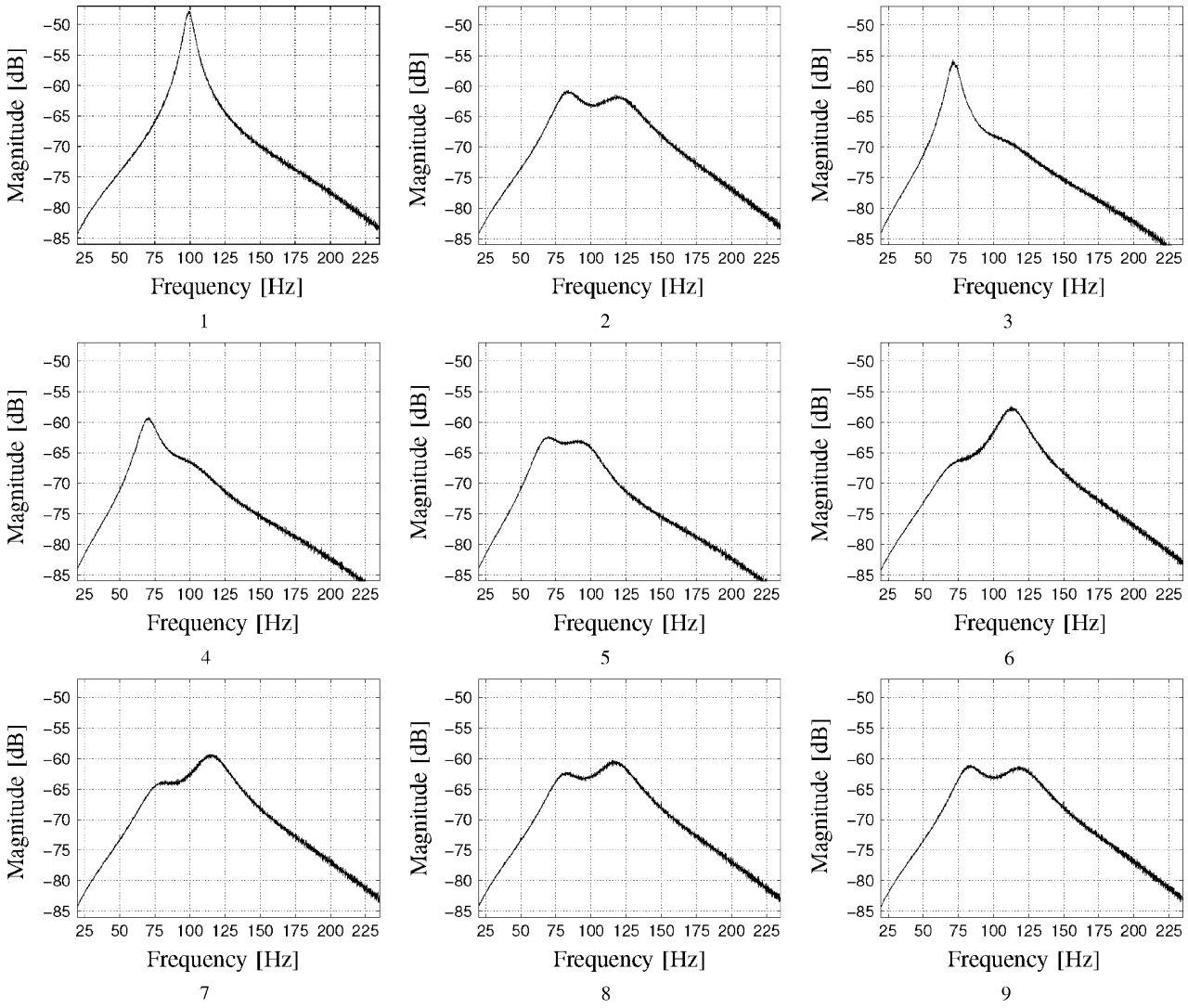

Fig. 7. Tuning using relative phase adaptation. The resonance frequency is changed by adding a small mass to the system and then removing it again.

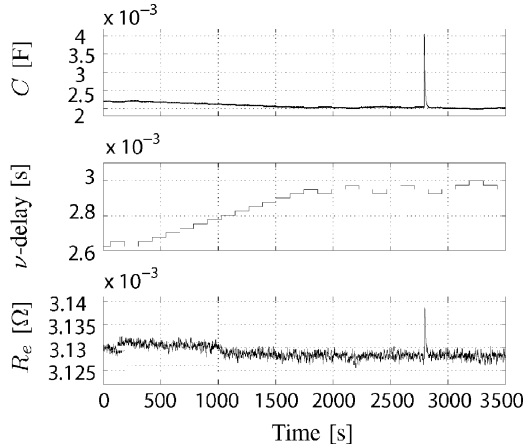

Fig. 8. Automatic setting of the compensator (ν-delay) for the relative phase adaptation.

The C–R adaptive shunt controller was verified experimentally on a electromagnetic mass spring damper system. A vibration suppression of 22.75 dB was obtained during nominal operating conditions. When subjected to induced changes in operating conditions, relative phase adaptation was found to converge seven times faster and display less misadjustment at the minimum. Although both techniques are simple in implementation, relative phase adaption requires an initial compensator setting. This can also be automated, if required.

REFERENCES

[1] S. S. Rao, *Mechanical Vibrations*, 3rd ed. Reading, MA: Addison-Wesley, 1995.

[2] B. M. Hanson, M. D. Brown, and J. Fisher, "Self sensing: closed-loop estimation for a linear electromagnetic actuator," in *Proc. IEEE Amer. Control Conf.*, Arlington, VA, 2001, pp. 1650–1655.

[3] S. Behrens, A. Fleming, and S. O. R. Moheimani, "Electromagnetic shunt damping," in *Proc. IEEE/ASME Int. Conf. Advanced Intelligent Mechatronics*, vol. 2, Kobe, Japan, 2003, pp. 1145–1150.

[4] Y. B. Kim, W. G. Hwang, C. D. Kee, and H. B. Yi, "Active vibration control of suspension system using an electromagnetic damper," in *Proc. Inst. Mech. Eng. D.-J. Automoblie Eng.*, vol. 215, 2001, pp. 865–873.

[5] J. Shaw, "Active vibration isolation by adaptive control," in *Proc. IEEE Int. Conf. on Control Applications*, Kohala Coast, Kamuela, HI, 1999, pp. 1509–1514.

[6] R. L. Forward, "Electronic damping of vibrations in optical structures," *Appl. Opt.*, vol. 18, no. 5, pp. 690–697, Mar. 1979.

[7] N. W. Hagood and A. Von Flotow, "Damping of structural vibrations with piezoelectric materials and passive electrical networks," *J. Sound Vib.*, vol. 146, no. 2, pp. 243–268, 1991.

[8] D. L. Edberg, A. S. Bicos, C. M. Fuller, J. J. Tracy, and J. S. Fechter, "Theoretical and experimental studies of a truss incorporating active members," *J. Int. Materials Syst. Structures*, vol. 3, pp. 333–347, 1992.

[9] C. R. Fuller, S. J. Elliott, and P. A. Nelson, *Active Control of Vibration*. New York: Academic, 1996.

[10] G. S. Agnes, "Active/passive piezoelectric vibration suppression," in *Proc. Int. Soc. Opt. Eng. (SPIE) Smart Structures and Materials, Passive Damping*, vol. 2193, San Diego, CA, May 1994, pp. 24–34.

[11] L. R. Corr and W. W. Clark, "Energy dissipation analysis of piezoceramic semi-active vibration control," *J. Intell. Mater. Syst. Structures*, vol. 12, pp. 729–736, 2002.

[12] C. L. Davis and G. A. Lesieutre, "An actively tuned solid-state vibration absorber using capacitive shunting of piezoelectric stiffness," *J. Sound and Vib.*, vol. 232, no. 3, pp. 601–617, 2000.

[13] A. J. Fleming and S. O. R. Moheimani, "Adaptive piezoelectric shunt damping," *J. Smart Mater. Structures*, vol. 12, pp. 36–48, Jan. 2003.

[14] D. Niederberger, M. Morari, and S. Pietrzko, "Adaptive resonant shunted piezoelectric devices for vibration suppression," in *Proc. Int. Soc. Opt. Eng. (SPIE) Smart Structures and Materials, Smart Structures and Integrated Systems*, vol. 5056, Mar. 2003, pp. 213–224.

[15] J. J. Hollkamp and T. F. Starchville, "A self-tuning piezoelectric vibration absorber," in *Proc. 35th AIAA/ASME/ASCE/AHS/ACS Structures, Structural Dynamics and Materials Conf.,* Hilton Head, NC, 1994, Paper 94-1790.

[16] J. J. Hollkamp, "Multimodal passive vibration suppression with piezoelectric materials and resonant shunts," *J. Intell. Mater. Syst. Structures*, vol. 5, pp. 49–56, 1994.

[17] D. Niederberger, A. J. Fleming, S. O. R. Moheimani, and M. Morari, "Adaptive multi-mode resonant piezoelectric shunt damping," *J. Smart Mater. Structures*, vol. 13, no. 4, pp. 1025–1035, Oct. 2004.

[18] A. J. Fleming, S. Behrens, and S. O. R. Moheimani, "Synthetic impedance for implementation of piezoelectric shunt-damping circuits," *Inst. Elect. Eng. Electron. Lett.*, vol. 36, no. 18, pp. 1525–1526, Aug. 2000.

Kinematic and Dynamic Models of a Tripod System With a Passive Leg

Z. M. Bi and Sherman Y. T. Lang

***Abstract*—In this paper, a new tripod system is proposed for the light-metal machining application, and its kinematic and dynamic models are studied. The new tripod system is a type of parallel kinematic machine with three degrees of freedom, and it uses a passive leg to increase system stiffness and eliminate the undesired end-effector motion along some axes. Both the direct and inverse kinematic problems are solved, and the dynamic problem is modeled by applying the Newton–Euler approach. A case study is provided to validate the kinematic and dynamic models and illustrate this new tripod design.**

***Index Terms*—Kinematics and dynamics, modeling, parallel kinematic machine (PKM), tripod.**

I. INTRODUCTION

Parallel kinematic machines (PKMs) have some significant advantages in comparison with serial robots: more rigidity and accuracy, higher load capacity, and simpler inverse kinematics for the real-time control. Many PKMs have been developed for various applications, such as aircraft simulator [1], telescopes [2], positional tracker [3], micromotion [4], and machining tools [5]–[8]. However, because design methodologies and technologies have not been well studied, most available PKMs are high-cost machines that provide less accuracy than conventional machines; therefore, more exploration is required to make PKMs widely attractive to industry [9].

Most of the machining operations are symmetric, and five degrees of freedom (DOF) can move a cutting tool to any point with any orientation in the workspace. A typical PKM needs five or less DOF; in particular, two or three DOF are adequate for many applications [9]. Besides, a PKM with two or three DOF can be combined advantageously with other mechanisms to provide more DOF [10], [11]. Therefore, study on a PKM with two or three DOF is meaningful and promising.

Various PKMs have been developed at the National Research Council Canada [11]–[14]. The development of the new tripod system is

Manuscript received August 27, 2003; revised June 24, 2004 and June 30, 2005. Recommended by Technical Editor M. Meng.

The authors are with the Integrated Manufacturing Technologies Institute, National Research Council Canada, London, ON N5Y 4V4, Canada (e-mail: Zhuming.Bi@nrc-cnrc.gc.ca; Sherman.Lang@nrc-cnrc.gc.ca).

Digital Object Identifier 10.1109/TMECH.2005.863362